Enhancing membrane tension promotes extracellular vesicle secretion

Xuemin Sun, Yuehua Yang,* and Hongyuan Jiang†
Department of Modern Mechanics, University of Science and Technology of China, Hefei, Anhui 230026, China

(Received 9 February 2026; revised 27 May 2026; accepted 22 June 2026; published 14 July 2026)

Extracellular vesicles (EVs) hold great promise in drug delivery, disease diagnosis, and treatment; however, the inability to control EVs biogenesis critically limits their therapeutic and diagnostic potential. Although regulatory mechanisms for biochemical cues have been extensively studied, the principles governing how diverse mechanical cues from the extracellular microenvironment orchestrate EV secretion are poorly understood, hindering the development of scalable production strategies. Here, we resolve this by introducing a theoretical model that identifies membrane reservoir depletion as a universal biophysical switch for EV release. We discover that EV secretion is directly activated by the depletion of the membrane reservoir and the consequent rise in membrane tension. This tension-mediated mechanism provides a unifying framework that reconciles disparate experimental observations under various biophysical perturbations, including cell spreading, osmotic shock, contractile perturbation, and substrate stiffening. Furthermore, we identify the membrane reservoir size as a key intrinsic parameter setting the threshold for mechanical activation of EV secretion, offering a rationale for engineering high-yield producer cell lines. Our work thus establishes a unifying mechanochemical framework for EV secretion, explaining disparate experimental observations and providing a quantitative design principle for optimizing EV production.

DOI: 10.1103/n6jp-gg95

I. INTRODUCTION

Extracellular vesicles (EVs) are lipid-bilayer-bound nanoparticles ubiquitously released by eukaryotic cells. They serve as vehicles encapsulating signaling molecules to participate in intercellular communication [1–4], operating alongside other highly diverse and critical physical pathways, such as tunneling nanotubes (TNTs) and other membranous nanovesicles [5–7]. Furthermore, dysfunctional EV secretion is implicated in a spectrum of diseases, such as neurodegenerative disorders [8–10], cancer [11–13], and diabetes [14,15]. Thus EVs hold immense promise in nanomedicine for drug delivery [16], diagnostics [17], and regenerative therapies [18,19], due to their biocompatibility, stability, and targeting capabilities. Harnessing this potential, however, requires precise control over EV biogenesis and release.

In the past decades, major efforts to achieve this control have predominantly relied on biochemical perturbations, such as targeting cytoskeletal dynamics or vesicle fusion machinery [20–22]. However, these methods are often hampered by inherent limitations, such as low spatial selectivity, complex side effects, and slow temporal response, making them suboptimal for the precise and scalable manufacturing of EV-based therapeutics. To overcome these challenges, there has been a growing focus on the use of physical forces as a potent and tunable alternative for controlling EV secretion. Emerging evidence demonstrates that diverse mechanical forces, such as shear force [23], osmotic pressure [24,25], stretching [26,27], compression [23,25], and substrate stiffness [28–31], can effectively regulate EV release. This positions biophysical stimulation as a promising frontier for engineering EV production. Despite these observations, a unifying principle that predicts how these disparate mechanical cues are integrated by the cell to control EV secretion is still lacking. Elucidating this regulatory mechanism is paramount, both for understanding cellular homeostasis and for developing effective EV-based therapies.

A central clue to this puzzle lies in the interplay between membrane tension and the membrane reservoir. Membrane tension is a key physical parameter that governs the energetic cost of membrane deformation during vesicle formation and fusion. Elevated membrane tension resists the deformation required for pore formation [32–34], thereby raising the energy barrier that SNARE proteins must overcome to drive vesicle fusion [35,36]. Conversely, cells possess a membrane reservoir, a pool of membrane wrinkles stored in folds, microvilli, and caveolae [37–41], that acts as a physical buffer, being incorporated upon mechanical perturbation to dampen tension rises and maintain mechanical homeostasis [42,43].

Here, we develop a theoretical framework that integrates cell adhesion, deformation, and membrane dynamics to decode the biophysical control of EV release. We demonstrate that diverse mechanical perturbations, including cell spreading, osmotic compression, active contraction, and substrate stiffening, are initially buffered by the membrane reservoir. Crucially, EV release is specifically triggered upon reservoir depletion, leading to a sharp increase in membrane tension. This mechanism unifies the cellular response to a wide spectrum of biophysical cues used in experiments. Our work thus

*Contact author: hz293033@ustc.edu.cn
†Contact author: jianghy@ustc.edu.cn

 ©2026 American Physical Society

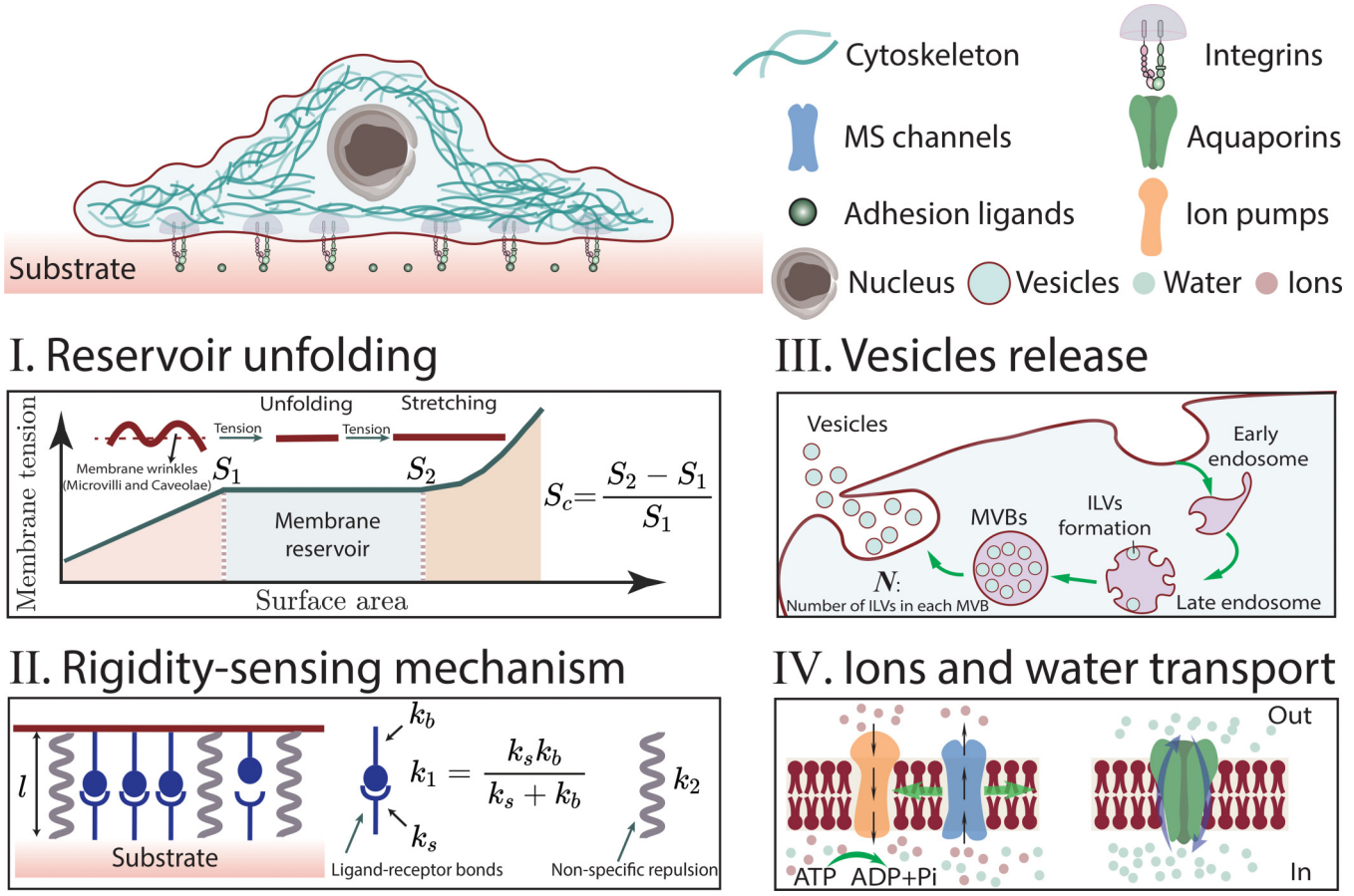

FIG. 1. Theoretical framework for mechanoregulated EV secretion. The model integrates four key cellular processes that couple mechanical stimuli to EV secretion via membrane tension. (I) Membrane reservoir dynamics: increased surface area initially unfolds membrane reservoirs to buffer tension (blue region), until reservoir depletion results in a sharp tension rise (orange region). The membrane reservoir activation threshold area (S_1), reservoir depletion threshold area (S_2), and normalized reservoir size (S_c) are defined. (II) Stiffness-sensing mechanism: cell-substrate adhesion is modeled via a two-spring system representing specific ligand-receptor bonds and nonspecific glycocalyx repulsion. Ligand-receptor bonds and substrate are modeled as two springs in series, with spring constant k_b (bond spring) and k_s (substrate spring), respectively. k_2 represents the equivalent spring constant of glycocalyx and l is the separation between cell membrane and the substrate. (III) Vesicle biogenesis and release: intraluminal vesicles (ILVs) are formed within multivesicular bodies (MVBs), which subsequently fuse with the plasma membrane to release vesicles. Here, N denotes the average number of ILVs per MVB. (IV) Ion and water transport: mechanosensitive (MS) channels (blue) open under elevated tension to permit ion flow down their concentration gradient, while active ion pumps (yellow) consume ATP to transport ions against their concentration gradient. Water movement is facilitated by aquaporins (green).

establishes a fundamental design principle for controlling the release of EV, explaining disparate experimental observations and providing a quantitative guide for optimizing EV production strategies.

II. METHODS

To investigate how diverse mechanical stimuli regulate extracellular vesicle release, we develop a theoretical model centered on the core hypothesis that membrane tension serves as a common integrator of mechanical cues, and the membrane reservoir is the key buffer controlling its dynamics. Our model couples four interconnected physiological processes (Fig. 1): (1) membrane reservoir unfolding induced by cell deformation, (2) the rigidity-sensing mechanism accounting for mechanosensing of substrate stiffness, (3) the vesicle release processes, and (4) water and ion transports. We integrate these processes as they collectively define the cellular mechanical state: adhesion and deformation (Process 1 and 2) alter the membrane area, which is buffered by the reservoir (Process 1) and ultimately transduced into a tensile signal that gates vesicle exocytosis (Process 3). Concurrently, osmotic forces and ion fluxes (Process 4) directly influence cell volume and pressure, providing an alternative pathway to modulate membrane tension and area.

A. Membrane reservoir and constitutive law

The mechanical behavior of the cell membrane undergoing deformations has been established by pioneering theoretical and experimental studies [44–47]. These classical works delineated a three-regime constitutive relationship [48–50]. Initially, the apparent membrane wrinkles and folds serve as a vast membrane reservoir [46]. This membrane reservoir buffers membrane tension increase. However, when the

wrinkles are smoothed out completely and the apparent membrane area reaches its maximal possible value (S_2), further increase of the area becomes exceedingly difficult, leading to sharp tension increase. This is because the lipid bilayer plasma membrane inherently shows very large resistance to area dilation [44,45], causing the tension T_m to rise sharply. According to these observations, we model membrane tension T_m as a function of cell surface area S

$$T_m = \begin{cases} E_m(S - S_r)/S_r & \text{if } S < S_1, \\ E_m(S_1 - S_r)/S_r & \text{if } S_1 \leqslant S \leqslant S_2, \\ E_m(S_1 - S_r)/S_r + E_n[e^{b_n(S-S_2)/S_r} - 1] & \text{if } S > S_2, \end{cases} \tag{1}$$

where E_m is the membrane elastic modulus in the linear phase and S_r is the reference area. The range of the membrane reservoir phase is defined by S_1 and S_2, which are the activation and depletion thresholds, respectively. The normalized reservoir size, defined as $S_c = S_2/S_1 - 1$, typically ranges between 1% and 30% [37,38,51]. The exponential term for $S > S_2$ is chosen to capture the dramatic stiffening of the lipid bilayer upon reservoir depletion. To ensure that the membrane becomes physically harder to stretch after depletion, the parameters are constrained such that the initial apparent modulus of the exponential phase exceeds the linear modulus, i.e., $b_n E_n \geqslant E_m$.

B. Dynamics of multivesicular bodies

EVs encompass various subclasses, primarily including exosomes [derived from the endosomal system via multivesicular bodies (MVBs)] and microvesicles (shed directly from the plasma membrane) [4,52]. In this study, we focus on modeling the dynamics of MVB-derived EVs (exosomes) to decode how diverse mechanical forces from the extracellular microenvironment orchestrate their secretion.

Multivesicular bodies (MVBs) fuse with the plasma membrane, releasing their intraluminal vesicles (ILVs) as EVs [19,53–55]. The number of MVBs evolves according to the balance of formation and fusion (see Supplemental Material [56] for details)

$$\frac{dM}{dt} = -V_{\text{re}} + V_f, \tag{2}$$

where V_{re} is the rate of MVBs fusion and V_f is the rate of MVBs formation. We assume the rate of MVBs fusion V_{re} is proportional to the number of MVBs (M) inside the cell $V_{\text{re}} = k_{\text{re}}M$, where k_{re} is the MVBs fusion rate. The fusion of MVBs with the plasma membrane typically occurs on the order of milliseconds (10^{-3} s) [81–83]. In contrast, the macroscopic cell spreading area and cell volume equilibrate on the order of 10^3–10^4 s [84–87], which is much longer than the timescale of MVBs fusion. Therefore, we treat MVB fusion as an instantaneous event and do not explicitly model fusion kinetics.

We next derive the rate equation for MVB formation using membrane energetics. Similar to previous studies [88,89], we consider a flat membrane as the initial state and the state in which the membrane invaginates to form an MVB as the final state. The difference in elastic potential energy between these two states is denoted by ΔE_{bend} [88,89]. In addition, there is the work done by membrane stretching during the MVB process, $W = T_m \Delta A$. Associated proteins also perform active work ($-W_a$). Together, the total change in energy is $\Delta E = \Delta E_{\text{bend}} - W_a + T_m \Delta A$. According to statistical mechanics, the probability of the membrane in the MVB state is $P_{\text{MVB}} = 1/[1 + \exp(\Delta E/k_B T)]$. Assuming a basal kinetic attempt frequency (k_f), the rate of MVB formation can be described by $V_f = k_f \cdot P_{\text{MVB}} = k_f/[1 + \exp(\Delta E/k_B T)]$. Substituting $\Delta E = \Delta E_{\text{bend}} - W_a + T_m \Delta A$ into the expression of MVB formation rate, we have

$$V_f = \frac{k_f}{1 + \exp\left(\frac{T_m - a}{b}\right)}, \tag{3}$$

where $a = (W_a - \Delta E_{\text{bend}})/\Delta A$ is a characteristic tension that describes the biophysical properties of the MVB formation process and $b = k_B T/\Delta A$ represents the width of the smooth transition caused by thermal fluctuations. This equation indicates that the formation rate of MVB decreases with tension, which is consistent with previous experimental observations [87,90–93]. We also find that the simulation results are qualitatively independent of the specific functional relationship between MVB formation rate and membrane tension (Fig. S2 in the Supplemental Material [56]).

The ILVs inside MVBs are secreted outside the cell once MVBs fuse with the plasma membrane. Thus the number of secreted vesicles n_v can be described as

$$\frac{dn_v}{dt} = NV_{\text{re}}, \tag{4}$$

where N is the average number of ILVs per single MVB.

C. Water and ions transport

As cells are open systems, they usually exchange water and ions with external environment under mechanical forces, leading to significant changes in cell volume, hydrostatic pressure, and membrane tension [85,94,95]. The cellular volume changes are related to water flux through the cell membrane [96] and volume changes caused by MVBs formation and fusion [42] and are given by

$$\frac{dV}{dt} = S_{\text{eff}} J_w + \frac{4}{3}\pi R_m^3 \frac{dM}{dt}, \tag{5}$$

where S_{eff} is the cell area through which water can pass and J_w is the flow rate of water across cell membrane per unit area (see [56] for details). The second term in the right side represents the transport of water via MVBs formation and fusion.

The number of ions inside cells is mainly related to three types of transport processes (Fig. 1 IV). First, ions can passively cross the membrane through mechanosensitive (MS)

channels, denoted as J_{ms}. Second, ion pumps actively transport ions against ion concentration gradients, denoted as J_{pump}. Third, cells can exchange ions with the extracellular environment through MVBs formation and fusion, denoted as J_{mvb}. Taking these three main processes into consideration, the change in the number of ions inside cells is given by

$$\frac{dn}{dt} = S_{\mathrm{eff}}(J_{\mathrm{ms}} + J_{\mathrm{pump}} + J_{\mathrm{mvb}}). \tag{6}$$

D. Rigidity-sensing mechanism and cell adhesion

To describe cellular sensing of substrate stiffness, we adopt an established two-spring framework [85,97,98] that describes how cells sense stiffness through adhesion dynamics (Fig. 1 II). Ligand-receptor bonds and substrate deformation are modeled as two springs in series, with stiffness values k_b (bond spring) and k_s (substrate spring), respectively. The equivalent spring stiffness is given by $k_1 = k_b k_s/(k_b + k_s)$ and its rest length is denoted l_1 (Fig. 1 II). In addition to ligand-receptor bonds, there are generally nonspecific repulsive forces between cells and substrates. For example, electrostatic forces originate from the glycocalyx [99]. These glycocalyx molecules can be modeled as springs with stiffness k_2 and rest length l_2 (Fig. 1 II).

Ligand-receptor bonds undergo stochastic binding and unbinding. Their density ρ_{lr} evolves as [76,100,101]

$$\frac{d\rho_{\mathrm{lr}}}{dt} = k_{\mathrm{on}}(\rho_r - \rho_{\mathrm{lr}}) - k_{\mathrm{off}}\rho_{\mathrm{lr}}, \tag{7}$$

where ρ_r is the total receptor density and k_{on} and k_{off} are the binding and dissociation rates, respectively. Unlike dynamic ligand-receptor bonds, these glycocalyx repellers are assumed to be immobile, with a constant area density equal to ρ_g [102].

The binding rate of ligand-receptor bonds k_{on} depends on the separation distance l between the cell and substrate and is given by [103,104]

$$k_{\mathrm{on}} = k_{\mathrm{on}}^0 \exp(-(l - l_1)^2/\lambda), \tag{8}$$

where k_{on}^0 is the rate constant and λ is a characteristic length scale. The dissociation rate k_{off} follows the classical two-pathway model [77,103,104]

$$k_{\mathrm{off}} = k_c^0 \exp(-a_c f/k_B T) + k_s^0 \exp(a_s f/k_B T), \tag{9}$$

where f is the average force per bond, k_c^0 and k_s^0 represent the unstressed ($f = 0$) dissociation rates of catch and slip bonds, respectively, and a_c and a_s are their characteristic lengths. k_B is the Boltzmann constant and T is the absolute temperature.

To couple this stiffness-sensing mechanism at the adhesion site to the global mechanical state of the cell, we employ the Young-Dupré equation describing cell-substrate adhesion:

$$\Gamma = T_m(1 - \cos\theta_0), \tag{10}$$

where Γ is the adhesion energy density, θ_0 is the contact angle, and T_s is the membrane tension. The adhesion energy density Γ includes two parts: a chemical term Γ_c and a mechanical term Γ_m [85,98,105], such that $\Gamma = \Gamma_c + \Gamma_m$. We take Γ_c as a constant. The mechanical term Γ_m is modeled as the total elastic energy stored in the bonds and repellers:

$$\Gamma_m = \tfrac{1}{2}\rho_{\mathrm{lr}}k_1(l - l_1)^2 + \tfrac{1}{2}\rho_g k_2(l - l_2)^2. \tag{11}$$

Combining the pulled forces from ligand-receptor bonds and the repulsive forces from glycocalyxs, the force equilibrium is described as $\rho_{\mathrm{lr}}k_1(l - l_1) + \rho_g k_2(l - l_2) = 0$, yielding the equilibrium length as $l = (\rho_{\mathrm{lr}}k_1 l_1 + \rho_g k_2 l_2)/(\rho_{\mathrm{lr}}k_1 + \rho_g k_2)$. Substituting this length into Eq. (11) leads to

$$\Gamma_m = \frac{1}{2}\frac{k_1 k_2 \rho_{\mathrm{lr}}\rho_g}{\rho_{\mathrm{lr}}k_1 + \rho_g k_2}(l_2 - l_1)^2. \tag{12}$$

III. RESULTS

A. Cell spread triggers EV release by depleting membrane reservoir

To establish a predictive framework for mechanically controlling EV release, we first investigate how cell spreading regulates vesicle release. We simulate the dynamic spreading of an initially spherical cell on a flat substrate. We find that both the normalized spreading area $\tilde{S}_a$ [Fig. 2(a)] and the cumulative EV release n_v [Fig. 2(b)] exhibit two distinct kinetic phases: a rapid initial increase followed by a slow saturation in area and a corresponding initial suppression followed by a sharp rise in vesicle release. These trends align well with previous experimental data [markers in Fig. 2(b)] [43,106,107]. We hypothesized that this kinetic transition is governed by depletion of the membrane reservoir and the resulting increase in membrane tension.

To test this hypothesis, we track membrane tension T_m during cell spreading [Fig. 2(c)]. The tension evolution exhibits the same biphasic regimes as n_v: an initial plateau where the reservoir buffers area increases without raising tension (blue region), followed by a steep rise upon reservoir exhaustion [brown region in Fig. 2(c)]. This transition occurs when the total membrane area S crosses the plateau of the tension-area constitutive curve (i.e., S_2 in Fig. 1 I), defining a critical threshold for activation.

The causal relationship between tension increase and EV release is unequivocally demonstrated in Fig. 2(d), where we plot vesicle output against the change in membrane tension. The data reveal a sharp, threshold-like response: vesicle release remains minimal during the initial buffering phase (data clustered near the origin), but surges exponentially once the tension exceeds a critical value upon reservoir depletion. This directly confirms that reservoir exhaustion is the trigger for tension-driven EV release.

To quantitatively establish the tension-release relationship, we plot vesicle output n_v against tension change $T_m - T_{m,0}$ [Fig. 2(d)]. The data reveal a sharp, threshold-like response: vesicle release remains minimal during the initial buffering phase (data clustered near the origin), but increases exponentially once the tension exceeds a critical value upon reservoir depletion. This directly confirms that reservoir exhaustion is the trigger for tension-driven EV release.

To further validate the reservoir's role as a tunable design parameter, we systematically varied its size S_c and examined its impact on EV release dynamics. A larger reservoir widens the plateau in the constitutive relation [Fig. S3(a) in the Supplemental Material [56]], thereby increasing the critical spreading area $S_{a,c}$ required to trigger vesicle release [Figs. 2(f) and 2(g)] and delaying the onset of vesicle release [Fig. 2(e)]. Consequently, cells with larger reservoirs

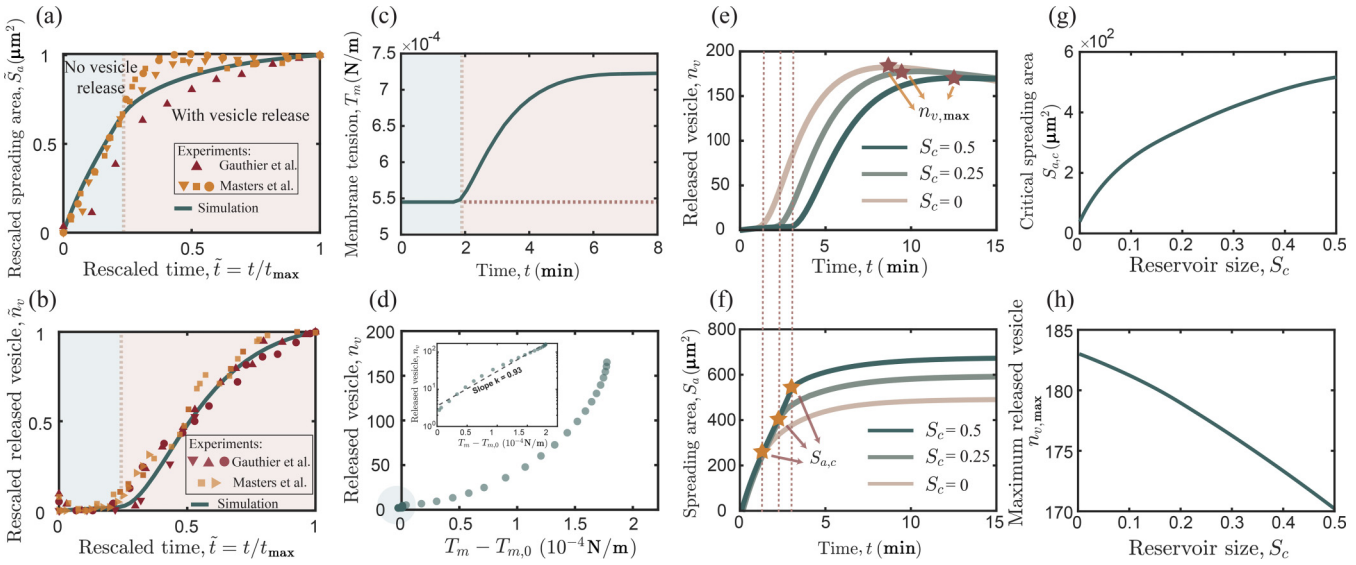

FIG. 2. Cell spreading triggers EV secretion by depleting membrane reservoir. (a) Time course of normalized cell spreading area (normalized by the maximum spreading area). Simulation results (lines) are compared with experimental data (points) from Gauthier *et al.* [43,106] and Masters *et al.* [107]. (b) Temporal changes in the number of released vesicles (rescaled with the maximum released number). (c) Evolution of membrane tension over time. (d) The number of released vesicles as a function of membrane tension change. Data in the inset is presented on a log-linear scale. (e) Changes in the number of released vesicles under different membrane reservoir sizes. (f) Evolution of spreading area under different membrane reservoir sizes. (g) Critical spreading area required to initiate vesicles release is plotted against reservoir size. (h) Correlation between the maximum number of released vesicles and membrane reservoir size.

exhibit attenuated tension increases and reduced vesicle release [Fig. 2(h)]. Similar trends are observed for total membrane area [Fig. S3(b) in the Supplemental Material [56]] and membrane tension [Fig. S3(c) in the Supplemental Material [56]]. These results demonstrate that reservoir size sets a cellular threshold for mechanosensitivity, governing both tension buffering and vesicle release kinetics.

B. Osmotic shocks directly gate EV release via membrane tension

The above results posit that an increase in membrane tension, consequent to reservoir depletion, is the proximate trigger for EV secretion. If this mechanism is universal, then elevating tension through an alternative physical perturbation should bypass the need for spreading-induced reservoir depletion and directly activate EV release.

To test this idea, we applied osmotic shocks to directly perturb tension independently of spreading-induced reservoir depletion. According to previous experiments [43,106,107], we apply a hypotonic shock with 50% reduction (i.e., $\Delta\tilde{\Pi}_{out} = \Delta\Pi_{out}/\Pi_{out} = -50\%$). Applying a hypotonic shock during the early spreading phase, prior to reservoir depletion [light blue region in Fig. 2(a)], induces an immediate burst of nanovesicle release, significantly advancing its initiation compared to the control [Fig. 3(b)]. This result aligns very well with previous experiments [43,106,107] and is explained by swelling-induced reservoir expansion and premature depletion [Figs. S4(b)–S4(d) in the Supplemental Material [56] in the Supplemental Material [56]]. Conversely, a hypertonic shock delays vesicle release [Fig. 3(f)], as water efflux caused membrane area reduction and tension decrease [Figs. 3(g) and 3(h) and Figs. S4(f) and S4(g) in the Supplemental Material [56]]. This bidirectional control confirms that osmotic perturbations regulate EV release through the tension-reservoir pathway.

Beyond osmotic shocks, a common experimental approach to regulate tension is pharmacological perturbation of active contractile forces [20–22]. We find that reducing active contraction promotes cell expansion and reservoir depletion, enhancing vesicle release, whereas enhancing active contraction leads to cell shrinkage, inhibiting vesicle release (Fig. S5) [56].

Collectively, these results establish membrane tension as a universal trigger and a tunable release gate for EV secretion. Whether raised by spreading, osmotic swelling, or contractility perturbation, elevated tension consistently prompts a burst of EV release.

C. Membrane reservoir sets a threshold for osmotic activation

Having established that osmotic shocks can directly control vesicle release by modulating the membrane reservoir, we next ask how the interplay between shock strength and reservoir size dictates the cellular response. Specifically, how can we precisely determine the stimulus strength required to overcome the reservoir's buffering capacity for optimal output?

Our analysis reveals that the efficiency of reservoir depletion, and consequently vesicle release, is programmable by both shock strength and reservoir size. A strong hypotonic shock with $\Delta\tilde{\Pi}_{out} = \Delta\Pi_{out}/\Pi_{out} = -50\%$ induces immediate and complete reservoir depletion [red line in Fig. 3(c)], facilitating rapid EV release. In contrast, a weaker hypotonic shock ($\Delta\tilde{\Pi}_{out} = -20\%$) results in only partial reservoir depletion [yellow line in 3(c)], thereby limiting release. Similarly, under hypertonic conditions, a larger shock

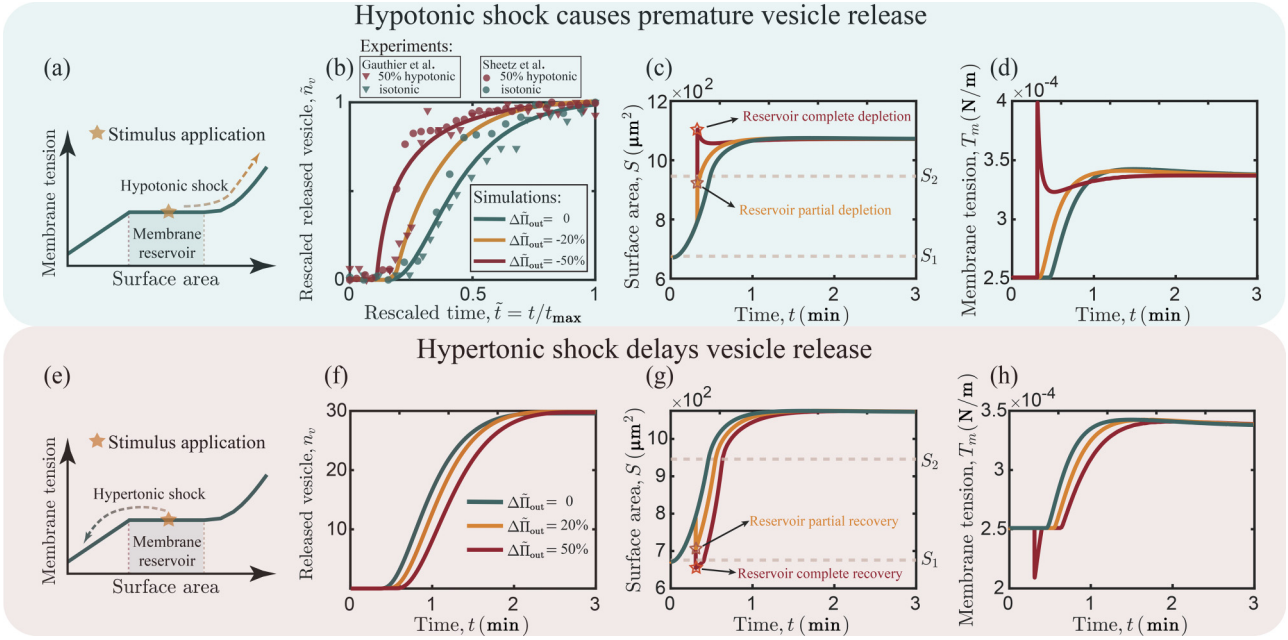

FIG. 3. Osmotic shocks modulate EV release through membrane tension. (a)–(d) Responses to hypotonic shock. (a) Water influx induced by the hypotonic shock to expand membrane reservoir, as depicted in the membrane constitutive schematic. Panels (b)–(d) show the temporal changes of vesicle release n_v, total membrane area S, and membrane tension T_m. Experimental data in (b) are from [43,106,107]. Different line colors indicate different shock amplitudes. (e)–(h) Responses to hypertonic shock. (e) Schematic diagram of cell shrinkage caused by hypertonic shock. (f)–(h) Temporal changes in vesicle release n_v (f), total membrane area S (g), and membrane tension T_m (h) under hypertonic shock.

($\Delta\tilde{\Pi}_{out} = 50\%$) fully restores the reservoir [red line in Fig. 3(g)], while a smaller shock ($\Delta\tilde{\Pi}_{out} = 20\%$) leads to only partial restoration [yellow line in Fig. 3(g)]. These observations demonstrate that a sufficiently strong osmotic stimulus is required for complete reservoir depletion or restoration.

To further validate this mechanism, we systematically characterize reservoir responses across a range of osmotic pressures and reservoir sizes, summarizing the results in phase diagrams (Fig. 4). Under hypotonic shocks, increasing the shock amplitude progressively shifts the system from partial to complete reservoir depletion [Fig. 4(a)]. Notably, the critical shock amplitude required for full reservoir depletion scales with reservoir size [Fig. 4(a), dashed line]. We further derive an analytical solution for this transition boundary: $\Delta\tilde{\Pi}_{out} = (1 + S_c)^{-3/2} - 1$ [circles in Fig. 4(a); see [56] for details], which aligns closely with simulation results. This relationship provides a quantitative criterion for selecting osmotic conditions necessary to deplete membrane reservoirs of varying sizes.

Conversely, under hypertonic shocks, the extent of membrane reservoir recovery is governed by both shock strength and initial reservoir size. Stronger shocks or smaller reservoirs favor complete recovery, whereas larger reservoirs require more intense stimuli to achieve full restoration [Fig. 4(b)]. This bidirectional control highlights the dynamic programmability of the membrane reservoir as a tunable release gate.

Collectively, these findings formalize the reservoir as a cellular thresholding device. The reservoir size sets a precise mechanical threshold that must be overcome by the stimulus (spreading or osmotic shock) to initiate the tensile rise required for triggering EV release.

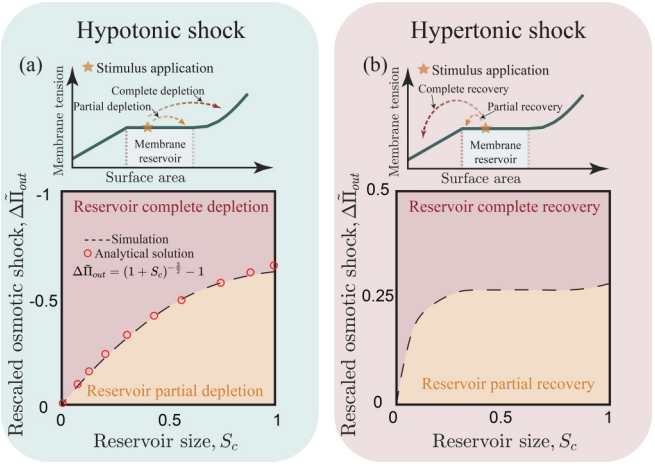

FIG. 4. Reservoir size dictates the shock strength required for membrane depletion and recovery. (a) Response to hypotonic shock. Top: schematics of cell surface area changes under different shock amplitudes. Bottom: state diagram depicting membrane reservoir depletion as a function of hypotonic shock strength and reservoir size. Red circles are the analytical solution for the transition boundary, where the expression is given in the figure. (b) Response to hypertonic shocks. Top: schematics of cell surface area changes under different shock amplitudes. Bottom: state diagram depicting membrane reservoir recovery as a function of hypertonic shock strength and reservoir size.

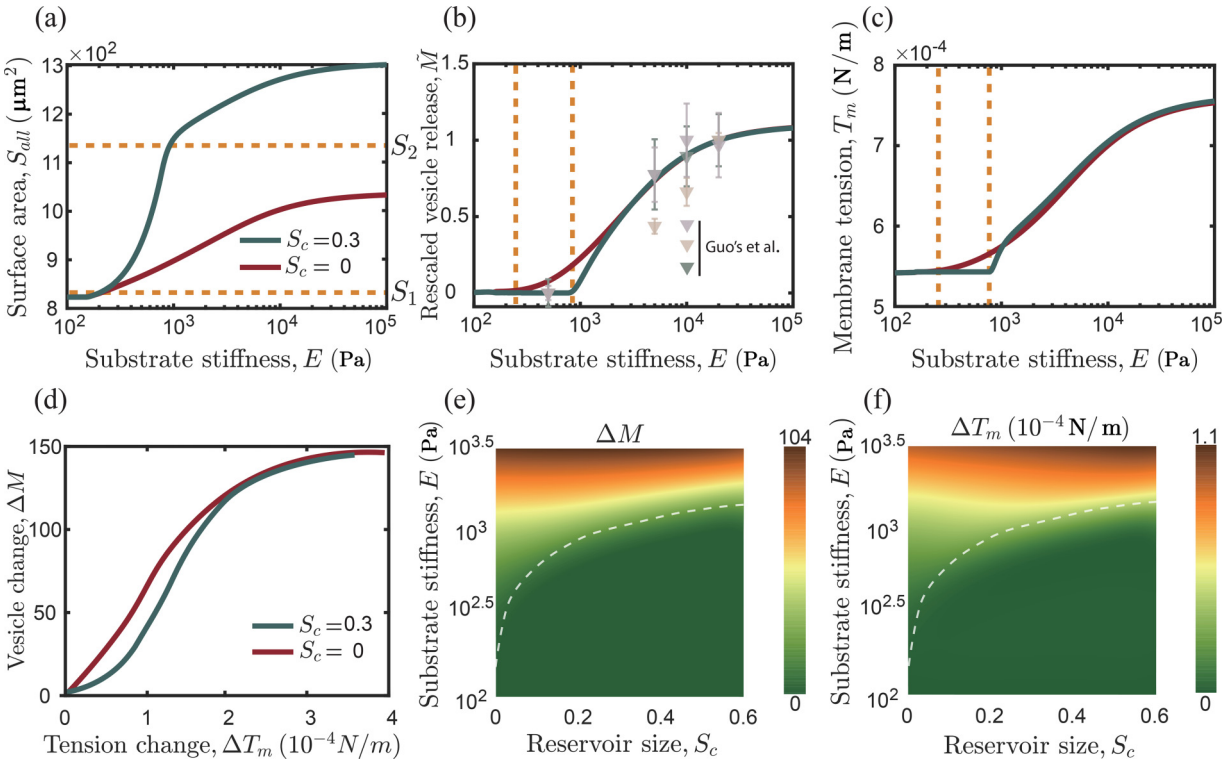

FIG. 5. Increasing substrate stiffness enhances EV release. (a)–(c) Stiffness-dependent changes in normalized cell surface area (a), vesicle release [(b), experimental data from Guo *et al.* [28]], and membrane tension (c) under distinct membrane reservoir sizes. (d) Correlation between the number of released vesicles and the corresponding changes in membrane tension. (e), (f) Heat maps of released vesicle count (e) and membrane tension changes (f) as a function of reservoir size and substrate stiffness.

D. Substrate stiffness promotes EV release through reservoir-dependent tension coupling

Recent experiments have shown that stiff substrate can promote EV secretion [28–31], however the underlying physical mechanics remain unclear. We speculate stiff substrate may also enhance EV release via depleting the membrane reservoir. To test this, we systematically vary substrate stiffness after cells reached steady-state adhesion and monitor the resulting mechanical and secretory responses.

We find that increasing substrate stiffness robustly enhances vesicle release [Fig. S6(a) in the Supplemental Material [56]]. This was accompanied by a rise in total membrane area [Fig. S6(b) in the Supplemental Material [56]] and a sustained increase in membrane tension [Fig. S6(c) in the Supplemental Material [56]]. These responses are consistently attenuated in cells with larger membrane reservoirs [Figs. S7(a)–S7(c) in the Supplemental Material [56]], confirming that the reservoir buffers stiffness-induced tension changes. Mechanistically, stiffer substrates promote stronger cell-substrate adhesion, which enhances cell spreading and accelerates reservoir depletion. As a result, membrane tension rises earlier and more strongly, triggering vesicle release. In contrast, cells with larger reservoirs require greater membrane expansion to initiate release, shifting the activation threshold toward higher stiffness [Fig. S7(d) in the Supplemental Material [56]].

At steady state, both total membrane area and tension change increase monotonically with substrate stiffness [Figs. 5(a)–5(c)], resulting in greater vesicle release, which is consistent with recent experiments [28–31]. Cells with a larger reservoir ($S_c = 0.3$) show suppressed EV secretion on soft substrates relative to reservoir-free cells ($S_c = 0$), though this buffering effect diminishes as stiffness increases [Fig. 5(b)], indicating that sufficiently stiff substrates can overwhelm the reservoir's buffering capacity. Notably, vesicle release correlates strongly with membrane tension across all conditions [Fig. 5(d)]. For a given level of release, cells with larger reservoirs require greater tension increases, underscoring the reservoir's role as a tension buffer and release gate.

To generalize these findings, we systematically map vesicle release and tension change as functions of both substrate stiffness and reservoir size [Figs. 5(d)–5(f)]. The critical stiffness required to initiate EV secretion and tension rise [marked by white dashed lines in Figs. 5(e) and 5(f)] increase with reservoir size, quantitatively confirming that the reservoir sets a mechanosensitive threshold for EV secretion.

Together, these results reveal that substrate stiffness is seamlessly incorporated into the reservoir-tension coupling framework. Stiffer substrates enhance cell spreading, deplete the reservoir more effectively, and elevate steady-state tension, thereby promoting EV release. The reservoir size again functions as a tunable design parameter, setting the stiffness threshold required to activate EV secretion.

E. Unified mechanism for mechanically stimulated EV release

Our model establishes that diverse mechanical stimuli, including cell spreading, osmotic shock, active contraction

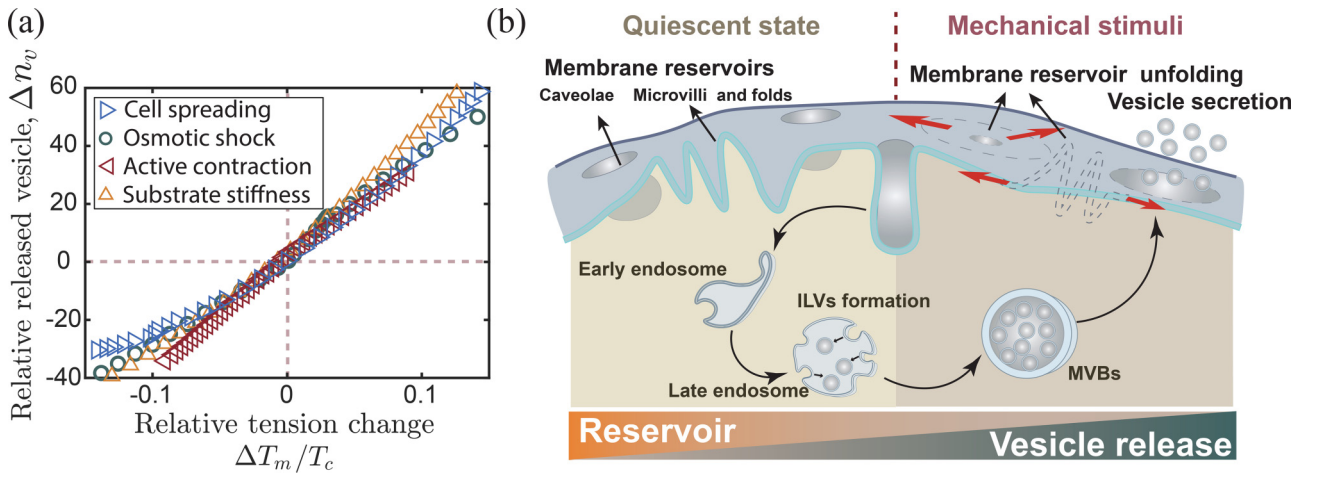

FIG. 6. Membrane reservoir depletion controls the mechanical activation of EV secretion. (a) The number of released vesicles scales with the amplitude of normalized membrane tension change. The dimensionless scaling of tension change is achieved by normalizing against the critical threshold tension T_c, where membrane reservoir is depleted. (b) The unified mechanism of vesicle release: mechanical stimuli deplete the membrane reservoir, leading to a rise in tension that subsequently induces EV secretion.

disturbance, and changes in substrate stiffness, regulate vesicle release through a common pathway involving the membrane reservoir. To unify these findings, we plot the change in membrane tension against vesicle release across all simulated conditions [Fig. 6(a)]. Strikingly, all data from diverse mechanical stimuli collapse onto a single master curve, demonstrating that EV output scales consistently with membrane tension regardless of the stimulus type [Fig. 6(a)]. This collapse provides compelling evidence that membrane tension is the central control variable for EV secretion [Fig. 6(b)].

IV. DISCUSSIONS

EVs are increasingly recognized not only as key mediators of intercellular communication [108,109] but also as a premier class of endogenous nanovesicles for therapeutic delivery [10,110–113]. While biochemical pathways regulating EV biogenesis have been extensively studied, the role of biophysical cues in modulating EV secretion remains poorly understood, hindering the development of robust, scalable production methodologies. Previous work has shown that individual mechanical force—such as spreading, osmotic shock, or substrate stiffness—can modulate EV secretion [28,43,114], yet a general, quantitative principle for predictable control has been missing. Here, we propose a unified framework in which membrane tension, gated by the membrane reservoir, serves as the central integrator of mechanical stimuli to control EV secretion from cells. This integrative view shows how distinct mechanical stimuli all converge onto the same tensile pathway, yielding a single predictive scaling relation between tension and vesicle output (Fig. 6).

A major challenge in fabricating EV-based drug carriers is the efficient and controllable formation of vesicles. Current EV-production platforms often apply mechanical stimuli empirically [114,115]. Our findings suggest that inducing and managing membrane tension via a simulated "reservoir-depletion" process could be a key to achieving on-demand cargo loading and release. For instance, in sequential microfluidic devices, an initial osmotic or mechanical "priming" step could be designed to deplete membrane reserves in precursor lipid bilayers, thereby sensitizing the system to a subsequent stimulus that triggers a synchronized burst of vesicle generation. This approach could move beyond current empirical methods [116–118] toward a tension-mediated programming of nanovesicle synthesis.

Our framework reveals that the membrane reservoir acts as a tunable mechanosensory threshold, quantitatively setting the cellular sensitivity to mechanical forces. This provides a cellular design principle for creating high-efficiency cell factories for EV production. Our model predicts that cells with a smaller inherent membrane reservoir or those in which reservoir components like caveolae are genetically down-regulated would exhibit a lower threshold for mechanical activation and consequently a higher secretory output. This prediction offers a rational strategy for cell line selection and engineering. Instead of relying on random genetic screening, one could prescreen candidate producer cells based on their reservoir abundance (e.g., via electron microscopy or specific biomarkers) and select those poised for high yield. Alternatively, genetically engineering cells to modulate the expression of microvilli, caveolae, or other reservoir constituents presents a powerful approach to customize EV production, optimizing cell platforms for industrial-scale EV production.

In summary, we identify the membrane reservoir as a universal mechanical buffer whose depletion gates vesicle release across a wide range of mechanical stimuli. And the membrane reservoir acts as a cellular thresholding device; only when mechanical inputs are sufficient to fully deplete the reservoir does tension rise sufficiently to trigger vesicle release. By identifying membrane reservoir depletion as a universal biophysical switch, our work not only reconciles disparate experimental observations but also establishes a quantitative and programmable framework for on-demand production of therapeutic nanovesicles.

ACKNOWLEDGMENTS

This work was supported by the National Natural Science Foundation of China (Grants No. 12532015, No. 12572363, No. 12372319, and No. 12025207), the Fundamental Research Funds for the Central Universities and USTC Research Funds of the Double First-Class Initiative (Grant No. YD2095202603). This work was partially carried out at the University of Science and Technology of China Center for Micro and Nanoscale Research and Fabrication.

Y.Y. and H.J. conceptualized the work; X.S. and Y.Y. conducted the model; X.S. performed the simulations; all authors wrote and reviewed the original draft.

DATA AVAILABILITY

The data that support the findings of this article are openly available at [119].

[1] F. M. Hughson, Both layers of the COPII coat come into view, Cell **134**, 384 (2008).

[2] M. Faini, R. Beck, F. T. Wieland, and J. A. Briggs, Vesicle coats: Structure, function, and general principles of assembly, Trends Cell Biol. **23**, 279 (2013).

[3] M. Faini, S. Prinz, R. Beck, M. Schorb, J. D. Riches, K. Bacia, B. Brügger, F. T. Wieland, and J. A. G. Briggs, The structures of COPI-coated vesicles reveal alternate coatomer conformations and interactions, Science **336**, 1451 (2012).

[4] M. Yáñez-Mó, P. R.-M. Siljander, Z. Andreu, A. Bedina Zavec, F. E. Borràs, E. I. Buzas, K. Buzas, E. Casal, F. Cappello, J. Carvalho, *et al.*, Biological properties of extracellular vesicles and their physiological functions, J. Extracell. Vesicles **4**, 27066 (2015).

[5] L. Mathivet, S. Cribier, and P. F. Devaux, Shape change and physical properties of giant phospholipid vesicles prepared in the presence of an AC electric field, Biophys. J. **70**, 1112 (1996).

[6] A. Rustom, R. Saffrich, I. Markovic, P. Walther, and H.-H. Gerdes, Nanotubular highways for intercellular organelle transport, Science **303**, 1007 (2004).

[7] P. Veranič, M. Lokar, G. J. Schütz, J. Weghuber, S. Wieser, H. Hägerstrand, V. Kralj-Iglič, and A. Iglič, Different types of cell-to-cell connections mediated by nanotubular structures, Biophys. J. **95**, 4416 (2008).

[8] C. P. Bravo, S. A. Naguib, and L. Gan, Cellular and pathological functions of tau, Nat. Rev. Mol. Cell Biol. **25**, 845 (2024).

[9] J. C. Polanco, C. Li, L.-G. Bodea, R. Martinez-Marmol, F. A. Meunier, and J. Götz, Amyloid-β and tau complexity — towards improved biomarkers and targeted therapies, Nat. Rev. Neurol. **14**, 22 (2018).

[10] C. Peng, J. Q. Trojanowski, and V. M.-Y. Lee, Protein transmission in neurodegenerative disease, Nat. Rev. Neurol. **16**, 199 (2020).

[11] B. Banushi, S. R. Joseph, B. Lum, J. J. Lee, and F. Simpson, Endocytosis in cancer and cancer therapy, Nat. Rev. Cancer **23**, 450 (2023).

[12] S. Sigismund, L. Lanzetti, G. Scita, and P. P. Di Fiore, Endocytosis in the context-dependent regulation of individual and collective cell properties, Nat. Rev. Mol. Cell Biol. **22**, 625 (2021).

[13] J. R. Goldenring, A central role for vesicle trafficking in epithelial neoplasia: Intracellular highways to carcinogenesis, Nat. Rev. Cancer **13**, 813 (2013).

[14] S. Yoon, A. Kovalenko, K. Bogdanov, and D. Wallach, MLKL, the protein that mediates necroptosis, also regulates endosomal trafficking and extracellular vesicle generation, Immunity **47**, 51 (2017).

[15] H. Xu, X. Du, G. Liu, S. Huang, W. Du, S. Zou, D. Tang, C. Fan, Y. Xie, Y. Wei, Y. Tian, and X. Fu, The pseudokinase MLKL regulates hepatic insulin sensitivity independently of inflammation, Mol. Metab. **23**, 14 (2019).

[16] I. K. Herrmann, M. J. A. Wood, and G. Fuhrmann, Extracellular vesicles as a next-generation drug delivery platform, Nat. Nanotechnol. **16**, 748 (2021).

[17] R. P. Carney, R. R. Mizenko, B. T. Bozkurt, N. Lowe, T. Henson, A. Arizzi, A. Wang, C. Tan, and S. C. George, Harnessing extracellular vesicle heterogeneity for diagnostic and therapeutic applications, Nat. Nanotechnol. **20**, 14 (2025).

[18] L. Cheng and A. F. Hill, Therapeutically harnessing extracellular vesicles, Nat. Rev. Drug Discovery **21**, 379 (2022).

[19] R. Kalluri and V. S. LeBleu, The biology, function, and biomedical applications of exosomes, Science **367**, eaau6977 (2020).

[20] I. Fujiwara, M. E. Zweifel, N. Courtemanche, and T. D. Pollard, Latrunculin A accelerates actin filament depolymerization in addition to sequestering actin monomers, Curr. Biol. **28**, 3183 (2018).

[21] T. A. McKinsey and D. A. Kass, Small-molecule therapies for cardiac hypertrophy: Moving beneath the cell surface, Nat. Rev. Drug Discovery **6**, 617 (2007).

[22] S. Pospich, F. Merino, and S. Raunser, Structural effects and functional implications of phalloidin and jasplakinolide binding to actin filaments, Structure **28**, 437 (2020).

[23] B. M. Gaub, K. C. Kasuba, E. Mace, T. Strittmatter, P. R. Laskowski, S. A. Geissler, A. Hierlemann, M. Fussenegger, B. Roska, and D. J. Müller, Neurons differentiate magnitude and location of mechanical stimuli, Proc. Natl. Acad. Sci. USA **117**, 848 (2020).

[24] M. Orlando, D. Schmitz, C. Rosenmund, and M. A. Herman, Calcium-independent exo-endocytosis coupling at small central synapses, Cell Rep. **29**, 3767 (2019).

[25] H. Ucar, S. Watanabe, J. Noguchi, Y. Morimoto, Y. Iino, S. Yagishita, N. Takahashi, and H. Kasai, Mechanical actions of dendritic-spine enlargement on presynaptic exocytosis, Nature (London) **600**, 686 (2021).

[26] W. W. Ahmed, T. C. Li, S. S. Rubakhin, A. Chiba, J. V. Sweedler, and T. A. Saif, Mechanical tension modulates local and global vesicle dynamics in neurons, Cell. Mol. Bioeng. **5**, 155 (2012).

[27] S. Siechen, S. Yang, A. Chiba, and T. Saif, Mechanical tension contributes to clustering of neurotransmitter vesicles at

presynaptic terminals, Proc. Natl. Acad. Sci. USA **106**, 12611 (2009).

[28] B. Wu, D.-A. Liu, L. Guan, P. K. Myint, L. Chin, H. Dang, Y. Xu, J. Ren, T. Li, Z. Yu, S. Jabban, G. B. Mills, J. Nukpezah, Y. H. Chen, E. E. Furth, P. A. Gimotty, R. G. Wells, V. M. Weaver, R. Radhakrishnan, X. W. Wang, *et al.*, Stiff matrix induces exosome secretion to promote tumour growth, Nat. Cell Biol. **25**, 415 (2023).

[29] D. Lachowski, C. Matellan, S. Gopal, E. Cortes, B. K. Robinson, A. Saiani, A. F. Miller, M. M. Stevens, and A. E. Del Río Hernández, Substrate stiffness-driven membrane tension modulates vesicular trafficking *via* Caveolin-1, ACS Nano **16**, 4322 (2022).

[30] Y. Wang, J. Wang, J. Zhang, Y. Wang, Y. Wang, H. Kang, W. Zhao, W. Bai, N. Miao, and J. Wang, Stiffness sensing via Piezo1 enhances macrophage efferocytosis and promotes the resolution of liver fibrosis, Sci. Adv. **10**, eadj3289 (2024).

[31] S. Patwardhan, P. Mahadik, O. Shetty, and S. Sen, ECM stiffness-tuned exosomes drive breast cancer motility through thrombospondin-1, Biomater. **279**, 121185 (2021).

[32] S. Boulant, C. Kural, J.-C. Zeeh, F. Ubelmann, and T. Kirchhausen, Actin dynamics counteract membrane tension during clathrin-mediated endocytosis, Nat. Cell Biol. **13**, 1124 (2011).

[33] X.-S. Wu, S. Elias, H. Liu, J. Heureaux, P. J. Wen, A. P. Liu, M. M. Kozlov, and L.-G. Wu, Membrane tension inhibits rapid and slow endocytosis in secretory cells, Biophys. J. **113**, 2406 (2017).

[34] W. Shin, L. Wei, G. Arpino, L. Ge, X. Guo, C. Y. Chan, E. Hamid, O. Shupliakov, C. K. Bleck, and L.-G. Wu, Preformed ω-profile closure and kiss-and-run mediate endocytosis and diverse endocytic modes in neuroendocrine chromaffin cells, Neuron **109**, 3119 (2021).

[35] M. Kaksonen and A. Roux, Mechanisms of clathrin-mediated endocytosis, Nat. Rev. Mol. Cell Biol. **19**, 313 (2018).

[36] N. Walani, J. Torres, and A. Agrawal, Endocytic proteins drive vesicle growth via instability in high membrane tension environment, Proc. Natl. Acad. Sci. USA **112**, E1423 (2015).

[37] B. Sinha, D. Köster, R. Ruez, P. Gonnord, M. Bastiani, D. Abankwa, R. V. Stan, G. Butler-Browne, B. Vedie, L. Johannes, N. Morone, R. G. Parton, G. Raposo, P. Sens, C. Lamaze, and P. Nassoy, Cells respond to mechanical stress by rapid disassembly of caveolae, Cell **144**, 402 (2011).

[38] C. G. Hansen and B. J. Nichols, Exploring the caves: Cavins, caveolins and caveolae, Trends Cell Biol. **20**, 177 (2010).

[39] J. L. Teo, G. A. Gomez, S. Weeratunga, E. M. Davies, I. Noordstra, S. Budnar, H. Katsuno-Kambe, M. J. McGrath, S. Verma, V. Tomatis, B. R. Acharya, L. Balasubramaniam, R. M. Templin, K.-A. McMahon, Y. S. Lee, R. J. Ju, S. J. Stebhens, B. Ladoux, C. A. Mitchell, B. M. Collins, *et al.*, Caveolae control contractile tension for epithelia to eliminate tumor cells, Dev. Cell **54**, 75 (2020).

[40] M. Štefl, M. Takamiya, V. Middel, M. Tekpınar, K. Nienhaus, T. Beil, S. Rastegar, U. Strähle, and G. U. Nienhaus, Caveolae disassemble upon membrane lesioning and foster cell survival, iScience **27**, 108849 (2024).

[41] R. Dharan, A. Barnoy, A. K. Tsaturyan, A. Grossman, S. Goren, I. Yosibash, D. Nachmias, N. Elia, R. Sorkin, and M. M. Kozlov, Intracellular pressure controls the propagation of tension in crumpled cell membranes, Nat. Commun. **16**, 91 (2025).

[42] F. Mao, Y. Yang, and H. Jiang, Endocytosis and exocytosis protect cells against severe membrane tension variations, Biophys. J. **120**, 5521 (2021).

[43] N. C. Gauthier, M. A. Fardin, P. Roca-Cusachs, and M. P. Sheetz, Temporary increase in plasma membrane tension coordinates the activation of exocytosis and contraction during cell spreading, Proc. Natl. Acad. Sci. USA **108**, 14467 (2011).

[44] E. Evans and B. Kukan, Passive material behavior of granulocytes based on large deformation and recovery after deformation tests, Blood **64**, 1028 (1984).

[45] E. A. Evans and R. Skalak, *Mechanics and Thermodynamics of Biomembranes*, 1st ed. (Taylor & Francis, London, 2018).

[46] G. W. Schmid-Schönbein, Leukocyte biophysics, Cell Biophys. **17**, 107 (1990).

[47] O. Thoumine, O. Cardoso, and J.-J. Meister, Changes in the mechanical properties of fibroblasts during spreading: A micromanipulation study, Eur. Biophys. J. **28**, 222 (1999).

[48] I. Titushkin and M. Cho, Distinct membrane mechanical properties of human mesenchymal stem cells determined using laser optical tweezers, Biophys. J. **90**, 2582 (2006).

[49] W. S. Rodenburg, S. F. A. Ebben, and J. M. Eeftens, Robust quantification of cellular mechanics using optical tweezers, Biophys. Rep. **5**, 100199 (2025).

[50] D. Raucher and M. P. Sheetz, Characteristics of a membrane reservoir buffering membrane tension, Biophys. J. **77**, 1992 (1999).

[51] P. Nassoy and C. Lamaze, Stressing caveolae new role in cell mechanics, Trends Cell Biol. **22**, 381 (2012).

[52] S. Fais, L. O'Driscoll, F. E. Borras, E. Buzas, G. Camussi, F. Cappello, J. Carvalho, A. C. Da Silva, H. Del Portillo, S. El Andaloussi, T. Ficko Trček, R. Furlan, A. Hendrix, I. Gursel, V. Kralj-Iglic, B. Kaeffer, M. Kosanovic, M. E. Lekka, G. Lipps, M. Logozzi, *et al.*, Evidence-based clinical use of nanoscale extracellular vesicles in nanomedicine, ACS Nano **10**, 3886 (2016).

[53] E. Cocucci and J. Meldolesi, Ectosomes and exosomes: Shedding the confusion between extracellular vesicles, Trends Cell Biol. **25**, 364 (2015).

[54] A. C. Dixson, T. R. Dawson, D. Di Vizio, and A. M. Weaver, Context-specific regulation of extracellular vesicle biogenesis and cargo selection, Nat. Rev. Mol. Cell Biol. **24**, 454 (2023).

[55] M. Colombo, G. Raposo, and C. Théry, Biogenesis, secretion, and intercellular interactions of exosomes and other extracellular vesicles, Annu. Rev. Cell Dev. Biol. **30**, 255 (2014).

[56] See Supplemental Material at http://link.aps.org/supplemental/10.1103/n6jp-gg95 for detailed model derivations, parameter values, a parameter table, and seven Supplemental Figures showing simulation results, which includes Refs. [42,57–80].

[57] A. Diz-Muñoz, D. A. Fletcher, and O. D. Weiner, Use the force: Membrane tension as an organizer of cell shape and motility, Trends Cell Biol. **23**, 47 (2013).

[58] G. Salbreux, G. Charras, and E. Paluch, Actin cortex mechanics and cellular morphogenesis, Trends Cell Biol. **22**, 536 (2012).

[59] M. P. Stewart, J. Helenius, Y. Toyoda, S. P. Ramanathan, D. J. Muller, and A. A. Hyman, Hydrostatic pressure and the

actomyosin cortex drive mitotic cell rounding, Nature (London) **469**, 226 (2011).

[60] S. Walcott and S. X. Sun, A mechanical model of actin stress fiber formation and substrate elasticity sensing in adherent cells, Proc. Natl. Acad. Sci. USA **107**, 7757 (2010).

[61] P. I. Hanson and A. Cashikar, Multivesicular body morphogenesis, Annu. Rev. Cell Dev. Biol. **28**, 337 (2012).

[62] R. Toriano, P. Ford, V. Rivarola, B. Tamarappoo, A. Verkman, and M. Parisi, Reconstitution of a regulated transepithelial water pathway in cells transfected with AQP2 and an AQP1/AQP2 hybrid containing the AQP2-C terminus, J. Membr. Biol. **161**, 141 (1998).

[63] M. Grosell, Intestinal anion exchange in marine fish osmoregulation, J. Exp. Biol. **209**, 2813 (2006).

[64] E. H. Larsen, N. Møbjerg, and R. Nielsen, Application of the Na^+ recirculation theory to ion coupled water transport in low- and high resistance osmoregulatory epithelia, Comp. Biochem. Physiol. A: Mol. Integr. Physiol. **148**, 101 (2007).

[65] K. Mitra, I. Ubarretxena-Belandia, T. Taguchi, G. Warren, and D. M. Engelman, Modulation of the bilayer thickness of exocytic pathway membranes by membrane proteins rather than cholesterol, Proc. Natl. Acad. Sci. USA **101**, 4083 (2004).

[66] J.-Y. Tinevez, U. Schulze, G. Salbreux, J. Roensch, J.-F. Joanny, and E. Paluch, Role of cortical tension in bleb growth, Proc. Natl. Acad. Sci. USA **106**, 18581 (2009).

[67] R. M. Hochmuth and N. Mohandas, Uniaxial loading of the red-cell membrane, J. Biomech. **5**, 501 (1972).

[68] T. G. Kuznetsova, M. N. Starodubtseva, N. I. Yegorenkov, S. A. Chizhik, and R. I. Zhdanov, Atomic force microscopy probing of cell elasticity, Micron Microscopy Nanobiotechnol. **38**, 824 (2007).

[69] S. T. Truschel, E. Wang, W. G. Ruiz, S.-M. Leung, R. Rojas, J. Lavelle, M. Zeidel, D. Stoffer, and G. Apodaca, Stretch-regulated exocytosis/endocytosis in bladder umbrella cells, Mol. Biol. Cell **13**, 830 (2002).

[70] P. Thorn, R. Zorec, J. Rettig, and D. J. Keating, Exocytosis in non-neuronal cells, J. Neurochem. **137**, 849 (2016).

[71] S. Bartnicki-Garcia, M. Garduño-Rosales, D. L. Delgado-Alvarez, and R. R. Mouriño-Pérez, Experimental measurement of endocytosis in fungal hyphae, Fungal Genetics Biol. **118**, 32 (2018).

[72] C. Villarroya-Beltri, F. Baixauli, M. Mittelbrunn, I. Fernández-Delgado, D. Torralba, O. Moreno-Gonzalo, S. Baldanta, C. Enrich, S. Guerra, and F. Sánchez-Madrid, ISGylation controls exosome secretion by promoting lysosomal degradation of MVB proteins, Nat. Commun. **7**, 13588 (2016).

[73] D. J. Katzmann, G. Odorizzi, and S. D. Emr, Receptor down-regulation and multivesicular-body sorting, Nat. Rev. Mol. Cell Biol. **3**, 893 (2002).

[74] F. J. Verweij, M. P. Bebelman, C. R. Jimenez, J. J. Garcia-Vallejo, H. Janssen, J. Neefjes, J. C. Knol, R. de Goeij-de Haas, S. R. Piersma, S. R. Baglio, M. Verhage, J. M. Middeldorp, A. Zomer, J. van Rheenen, M. G. Coppolino, I. Hurbain, G. Raposo, M. J. Smit, R. F. Toonen, G. van Niel, *et al.*, Quantifying exosome secretion from single cells reveals a modulatory role for GPCR signaling, J. Cell Biol. **217**, 1129 (2018).

[75] D. A. Hammer and S. M. Apte, Simulation of cell rolling and adhesion on surfaces in shear flow: General results and analysis of selectin-mediated neutrophil adhesion, Biophys. J. **63**, 35 (1992).

[76] C. Y. Zhang, Computational analysis of adhesion force in the indentation of cells using atomic force microscopy, Phys. Rev. E **77**, 021912 (2008).

[77] Y. V. Pereverzev, O. V. Prezhdo, M. Forero, E. V. Sokurenko, and W. E. Thomas, The two-pathway model for the catch-slip transition in biological adhesion, Biophys. J. **89**, 1446 (2005).

[78] T. Erdmann and U. S. Schwarz, Stability of adhesion clusters under constant force, Phys. Rev. Lett. **92**, 108102 (2004).

[79] L. Sun, Q. H. Cheng, H. J. Gao, and Y. W. Zhang, Effect of loading conditions on the dissociation behaviour of catch bond clusters, J. R. Soc., Interface **9**, 928 (2012).

[80] E. Puklin-Faucher, M. Gao, K. Schulten, and V. Vogel, How the headpiece hinge angle is opened: New insights into the dynamics of integrin activation, J. Cell Biol. **175**, 349 (2006).

[81] M. Lindau and G. A. de Toledo, The fusion pore, Biochim. Biophys. Acta (BBA) - Mol. Cell Res. **1641**, 167 (2003).

[82] C. Morris and U. Homann, Cell surface area regulation and membrane tension, J. Membr. Biol. **179**, 79 (2001).

[83] J. C. Shillcock and R. Lipowsky, Tension-induced fusion of bilayer membranes and vesicles, Nat. Mater. **4**, 225 (2005).

[84] L. Venkova, A. S. Vishen, S. Lembo, N. Srivastava, B. Duchamp, A. Ruppel, A. Williart, S. Vassilopoulos, A. Deslys, J. M. Garcia Arcos, A. Diz-Muñoz, M. Balland, J.-F. Joanny, D. Cuvelier, P. Sens, and M. Piel, A mechano-osmotic feedback couples cell volume to the rate of cell deformation, eLife **11**, e72381 (2022).

[85] K. Xie, Y. Yang, and H. Jiang, Controlling cellular volume via mechanical and physical properties of substrate, Biophys. J. **114**, 675 (2018).

[86] T. L. Nagy, E. Strickland, and O. D. Weiner, Neutrophils actively swell to potentiate rapid migration, eLife **12**, RP90551 (2024).

[87] J. Lemière, Y. Ren, and J. Berro, Rapid adaptation of endocytosis, exocytosis, and eisosomes after an acute increase in membrane tension in yeast cells, eLife **10**, e62084 (2021).

[88] V. Kralj-Iglic and V. Kralj-Iglic, Stability of membranous nanostructures: A possible key mechanism in cancer progression, Int. J. Nanomed. **2012**, 3579 (2012).

[89] V. Kralj-Iglič, G. Pocsfalvi, L. Mesarec, V. Šuštar, H. Hägerstrand, and A. Iglič, Minimizing isotropic and deviatoric membrane energy – an unifying formation mechanism of different cellular membrane nanovesicle types, PLoS One **15**, e0244796 (2020).

[90] T. Kirchhausen, Bending membranes, Nat. Cell Biol. **14**, 906 (2012).

[91] U. Djakbarova, Y. Madraki, E. T. Chan, and C. Kural, Dynamic interplay between cell membrane tension and clathrin-mediated endocytosis, Biol. Cell **113**, 344 (2021).

[92] K. E. Cavanaugh, M. F. Staddon, E. Munro, S. Banerjee, and M. L. Gardel, RhoA mediates epithelial cell shape changes via mechanosensitive endocytosis, Dev. Cell **52**, 152 (2020).

[93] L. A. Cingolani and Y. Goda, Actin in action: The interplay between the actin cytoskeleton and synaptic efficacy, Nat. Rev. Neurosci. **9**, 344 (2008).

[94] Y. Yang and H. Jiang, Shape and dynamics of adhesive cells: Mechanical response of open systems, Phys. Rev. Lett. **118**, 208102 (2017).

[95] C. Roffay, G. Molinard, K. Kim, M. Urbanska, V. Andrade, V. Barbarasa, P. Nowak, V. Mercier, J. García-Calvo, S. Matile, *et al.*, Passive coupling of membrane tension and cell volume during active response of cells to osmosis, Proc. Natl. Acad. Sci. USA **118**, e2103228118 (2021).

[96] H. Jiang and S. X. Sun, Cellular pressure and volume regulation and implications for cell mechanics, Biophys. J. **105**, 609 (2013).

[97] U. S. Schwarz, T. Erdmann, and I. B. Bischofs, Focal adhesions as mechanosensors: The two-spring model, Biosystems **83**, 225 (2006).

[98] X. Peng, J. Huang, C. Xiong, and J. Fang, Cell adhesion nucleation regulated by substrate stiffness: A Monte Carlo study, J. Biomech. **45**, 116 (2012).

[99] G. I. Bell, M. Dembo, and P. Bongrand, Cell adhesion: Competition between nonspecific repulsion and specific bonding, Biophys. J. **45**, 1051 (1984).

[100] C. E. Chan and D. J. Odde, Traction dynamics of filopodia on compliant substrates, Science **322**, 1687 (2008).

[101] Y. Lin and L. B. Freund, Forced detachment of a vesicle in adhesive contact with a substrate, Int. J. Solids Struct. **44**, 1927 (2007).

[102] J. Wang and H. Gao, Clustering instability in adhesive contact between elastic solids via diffusive molecular bonds, J. Mech. Phys. Solids **56**, 251 (2008).

[103] H. Jiang, J. Qian, Y. Lin, Y. Ni, and L. He, Aggregation dynamics of molecular bonds between compliant materials, Soft Matter **11**, 2812 (2015).

[104] S. Yu, H. Wang, Y. Ni, L. He, M. Huang, Y. Lin, J. Qian, and H. Jiang, Tuning interfacial patterns of molecular bonds via surface morphology, Soft Matter **13**, 5970 (2017).

[105] J. Huang, X. Peng, C. Xiong, and J. Fang, Influence of substrate stiffness on cell–substrate interfacial adhesion and spreading: A mechano-chemical coupling model, J. Colloid Interface Sci. **355**, 503 (2011).

[106] N. C. Gauthier, O. M. Rossier, A. Mathur, J. C. Hone, and M. P. Sheetz, Plasma membrane area increases with spread area by exocytosis of a GPI-anchored protein compartment, Mol. Biol. Cell **20**, 3261 (2009).

[107] T. A. Masters, B. Pontes, V. Viasnoff, Y. Li, and N. C. Gauthier, Plasma membrane tension orchestrates membrane trafficking, cytoskeletal remodeling, and biochemical signaling during phagocytosis, Proc. Natl. Acad. Sci. USA **110**, 11875 (2013).

[108] J. Meldolesi, Exosomes and ectosomes in intercellular communication, Curr. Biol. **28**, R435 (2018).

[109] G. Van Niel, D. R. F. Carter, A. Clayton, D. W. Lambert, G. Raposo, and P. Vader, Challenges and directions in studying cell–cell communication by extracellular vesicles, Nat. Rev. Mol. Cell Biol. **23**, 369 (2022).

[110] E. E. Congdon, C. Ji, A. M. Tetlow, Y. Jiang, and E. M. Sigurdsson, Tau-targeting therapies for Alzheimer disease: Current status and future directions, Nat. Rev. Neurol. **19**, 715 (2023).

[111] K. Iqbal, F. Liu, and C.-X. Gong, Tau and neurodegenerative disease: The story so far, Nat. Rev. Neurol. **12**, 15 (2016).

[112] Y. Wang and E. Mandelkow, Tau in physiology and pathology, Nat. Rev. Neurosci. **17**, 22 (2016).

[113] R. J. Mead, N. Shan, H. J. Reiser, F. Marshall, and P. J. Shaw, Amyotrophic lateral sclerosis: A neurodegenerative disorder poised for successful therapeutic translation, Nat. Rev. Drug Discovery **22**, 185 (2023).

[114] S. Wan, K. Wang, P. Huang, X. Guo, W. Liu, Y. Li, J. Zhang, Z. Li, J. Song, W. Yang, X. Zhang, X. Ding, D. T. Leong, and L. Wang, Mechanoelectronic stimulation of autologous extracellular vesicle biosynthesis implant for gut microbiota modulation, Nat. Commun. **15**, 3343 (2024).

[115] X. Yuan, J. Shi, Y. Kang, J. Dong, Z. Pei, and X. Ji, Piezoelectricity, pyroelectricity, and ferroelectricity in biomaterials and biomedical applications, Adv. Mater. **36**, 2308726 (2024).

[116] M. Peng, Q. Zhao, A. Chai, Y. Wang, M. Wang, and X. Du, A ferroelectric living interface for fine-tuned exosome secretion toward physiology-mimetic neurovascular remodeling, Matter **8**, 101901 (2025).

[117] A. Fang, Y. Wang, N. Guan, Y. Zuo, L. Lin, B. Guo, A. Mo, Y. Wu, X. Lin, W. Cai, X. Chen, J. Ye, Z. Abdelrahman, X. Li, H. Zheng, Z. Wu, S. Jin, K. Xu, Y. Huang, X. Gu, *et al.*, Porous microneedle patch with sustained delivery of extracellular vesicles mitigates severe spinal cord injury, Nat. Commun. **14**, 4011 (2023).

[118] S. Fu, Z. Wang, P. Huang, G. Li, J. Niu, Z. Li, G. Zu, P. Zhou, L. Wang, D. T. Leong, and X. Ding, Programmable production of bioactive extracellular vesicles in vivo to treat myocardial infarction, Nat. Commun. **16**, 2924 (2025).

[119] SUN-sysu-del, SUN-sysu-del/code-for-vesicles-realese-model: first stable release, Version V2.0.0 [Computer software], Zenodo, 2025, https://zenodo.org/records/17875760.